Separation Science and Technology
Publication details, including instructions for authors and subscription information:
http://www.informaworld.com/smpp/title~content=t713708471

Development of a Simulation Model Predicting Performance of Reverse Osmosis Batch Systems

C. S. Slater[a]; C. A. Brooks III[a]
[a] CHEMICAL ENGINEERING DEPARTMENT, MANHATTAN COLLEGE RIVERDALE, NEW YORK

To cite this Article Slater, C. S. and Brooks III, C. A.(1992) 'Development of a Simulation Model Predicting Performance of Reverse Osmosis Batch Systems', Separation Science and Technology, 27: 11, 1361 — 1388
To link to this Article: DOI: 10.1080/01496399208019431
URL: http://dx.doi.org/10.1080/01496399208019431

SEPARATION SCIENCE AND TECHNOLOGY, 27(11), pp. 1361–1388, 1992

Development of a Simulation Model Predicting Performance of Reverse Osmosis Batch Systems

C. S. SLATER and C. A. BROOKS III
CHEMICAL ENGINEERING DEPARTMENT
MANHATTAN COLLEGE
RIVERDALE, NEW YORK 10471

Abstract

A model describing concentration profiles and performance relationships for the operation of a reverse osmosis system with a spiral-wound membrane module has been developed. The model is an enhancement of a previously proposed treatment and encompasses a discussion of mass transfer relationships and overall and component mass balances on a system operating in a closed-loop concentrating or recycling pattern. The presentation of mass transfer within a spiral wound membrane module is treated with an overall module approach with solution-diffusion mass transfer parameters empirically determined. A comparison with various methods to represent membrane feed side concentration and their effect on membrane performance is presented. A perspective is made on representing concentration polarization in this type of membrane configuration. The simulation model is verified with experimental data on simple aqueous salt systems. The simulations are excellent in predicting feed concentration profiles. Permeate flux deviates moderately and the permeate concentration only deviates significantly at high recoveries. A more exact depiction of the feed-side concentration improves the correlation to experimental data, but a more simplistic treatment may suffice under certain process conditions. The concentration polarization coefficient utilized was found to depend more heavily on the increase in flux due to a decrease in feed-side concentration rather than in the direct increase in feed concentration.

INTRODUCTION

Reverse osmosis (RO) is a process which uses a semipermeable membrane to separate and/or concentrate a process stream. The growing interest in reverse osmosis has resulted because of the great promise it holds for performing separations more efficiently and economically. Reverse osmosis is presently utilized in water purification, chemical separations, and wastewater treatment (*1*). The majority of applications are in water purification, primarily the desalination of seawater and brackish water.

These applications are used for potable water production, and reverse osmosis is also used to produce ultrapure water for the electronics and pharmaceutical industries. Reverse osmosis has been extensively used to treat industrial wastewater and has been used in both standard end-of-pipe treatment systems and for reuse and recovery applications. Industrial waste renovation applications can be found in the chemical, textile, pulp and paper, electrochemical, pharmaceutical, and petrochemical industries (*1*, *2*). Reverse osmosis technology has also been employed for product concentration in the food, beverage, and dairy industries.

The application of reverse osmosis to specific process separations generally requires pilot-scale testing. Individual applications are often unique, and mass transfer aspects of membranes must be thoroughly understood in order to determine system performance and efficiency. This is particularly true in the purification of complex industrial wastewaters. The experimental methodology involves determining the relationships between the solvent flux and solute flux, and the pressure driving force and concentration driving force (*3*).

THEORY

Basic Mass Transfer

A reverse osmosis membrane is a thin, nonporous, semipermeable barrier separating two fluids that permits selective transport of certain species through the membrane from one fluid to the other. The solvent, which for reverse osmosis is usually water, is preferentially sorbed into the membrane, while other components (usually low molecular weight salts) are only slightly sorbed. The sorbed components move through the membrane at different rates by diffusion. The mechanism of selective permeation makes possible the separation of various components.

The flow of solvent through the membrane is defined in terms of a flux. The expression for the volumetric flux, J'_w, is

$$J'_w = Q_p/S_a \tag{1}$$

where Q_p is the volumetric flow rate of the permeate and S_a is the membrane surface area. The expression for the mass flux, J_w, is

$$J_w = \left(\frac{Q_p}{S_a}\right)C_d \tag{2a}$$

where C_d is the solvent permeate concentration or density, and for simplicity, is taken to be that of pure water (1000 kg/m^3). This is a valid assumption since the experimental studies described herein use aqueous solutions with high rejecting membranes. Equation (2a) can then be expressed as

$$J_w = \left(\frac{Q_p}{S_a}\right) C_w \tag{2b}$$

where C_w now represents the concentration of water.

Many models exist that describe the mass transport through reverse osmosis membranes. Several sources are available that detail the development that follows (*4–8*). According to the fundamental phenomenological transport expression, membrane transport occurs at a rate corresponding to the applied pressure and individual concentration gradients across the membrane. The following transport expressions were chosen for their simplicity since they utilize only two model constants.

The solvent flux, J_w, is proportional to the difference between the hydraulic pressure applied across the membrane and the osmotic pressure difference between the feed and permeate sides of the membrane:

$$J_w = A_w(\Delta P - \Delta\pi) \tag{3}$$

where A_w is the solvent or water permeability coefficient, and $\Delta\pi$ and ΔP are the hydraulic and osmotic pressure differences.

The solute flux, J_s, is proportional to the concentration gradient and is expressed as

$$J_s = B_s \Delta C \tag{4}$$

where J_s is a mass flux and B_s is the solute permeability coefficient. The difference in solute concentration across the membrane, ΔC, is expressed as

$$\Delta C = C_f^w - C_p \tag{5}$$

where C_f^w is the concentration in the boundary layer on the feed side of the membrane and C_p is the concentration of the permeate leaving the membrane. The concentration at the membrane surface, C_f^w, will be referred to as concentration at the wall to be consistent with other types of mass transfer analyses.

System Performance Relationships

A number of different expressions are often used to represent system performance. The concentration factor, CF, relates the feed concentration, after closed-loop batch processing, to the initial feed concentration. The relation is expressed as

$$\mathrm{CF} = C_f/C_f^0 \tag{6}$$

The recovery is a production term which relates permeate and feed flows,

$$Y = Q_p/Q_f \tag{7a}$$

Recovery for the overall system, operating in a closed-loop batch concentrating mode, is the total volume of permeate generated up to a given time divided by the initial feed volume:

$$X = V_p/V_f^0 \tag{7b}$$

The relationships between the feed, retentate, and permeate concentrations are often expressed as a membrane rejection. In terms of the feed and permeate concentrations, R is

$$R = \frac{C_f - C_p}{C_f} = 1 - \frac{C_p}{C_f} \tag{8a}$$

Rejection, R', in terms of the retentate and permeate concentrations, is

$$R' = \frac{C_r - C_p}{C_r} = 1 - \frac{C_p}{C_r} \tag{8b}$$

Rejection, R'', in terms of the feed, retentate, and permeate concentrations, is

$$R'' = \frac{(C_f + C_r)/2 - C_p}{(C_f + C_r)/2} = 1 - \frac{C_p}{(C_f + C_r)/2} \tag{8c}$$

This expression for R'' is specific to flow through membrane modules (e.g., tubular and spiral-wound membranes) where the feed concentration is expressed as an average of the feed entering and the retentate leaving. The recovery, Y, can be incorporated into the rejection equation. This is

a more exact representation for the rejection and is expressed as

$$R''' = 1 - \frac{\log (1 - Y(C_p/C_f))}{\log (1 - Y)} \tag{8d}$$

Concentration Polarization

Thus far, mass transfer has been considered to occur ideally. The flux inhibiting effects of concentration polarization and membrane fouling can greatly reduce the efficiency of a reverse osmosis system. Concentration polarization results from an increase in solute concentration at the membrane wall as compared to that of the bulk feed concentration (Fig. 1).

At steady-state conditions, solute is assumed not to accumulate on the membrane. Solute transport by diffusion away from the membrane surface must occur simultaneously with convective diffusion toward the membrane (*5*). This process is summarized by the following mass balance,

$$-J'_w(C_f) + D\frac{dc}{dy} = -J'_w(C_p) \tag{9}$$

where D is the diffusion coefficient of solute in solvent. The boundary conditions for the equation are:

at $y = 0$ (surface), $C_f = C_f^w$ (wall concentration)

at $y = l$ (edge of boundary layer), $C_f = C_f^b$ (bulk concentration)

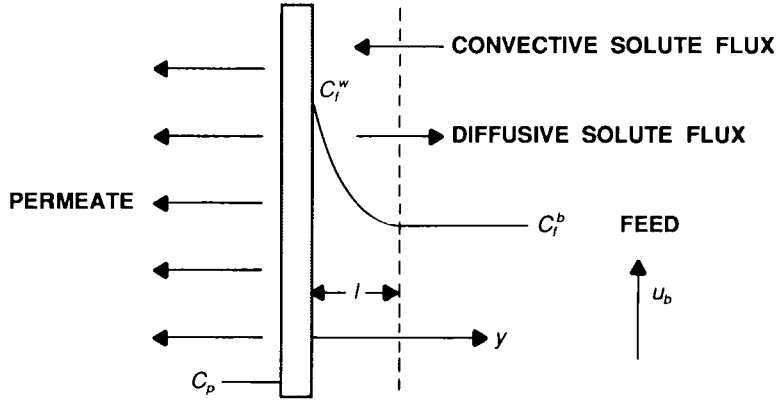

FIG. 1. Concentration polarization diagram.

The equation representing the mass balance has been solved with the given boundary conditions to give a relationship between operating variables (flux and rejection) and wall concentration, C_f^w, in terms of the boundary layer thickness (9).

$$\frac{C_f^w}{C_f^b} = \frac{\exp(J_w l/D)}{R_i + (1 - R_i)\exp(J_w l/D)} \tag{10}$$

where R_i is the intrinsic rejection as given by

$$R_i = 1 - \frac{C_p}{C_f^w} \tag{11}$$

The quantification of concentration polarization, as given by the ratio C_f^w/C_f^b, is specific to the flat plate geometry in Fig. 1. Because the geometries in a spiral-wound or hollow-fiber membrane module are more complex (Fig. 2), the ratio C_f^w/C_f^b is extremely difficult to quantify analytically. This facilitates the use of an overall module analysis where a "total" value of C_f^w/C_f^b for the system, i.e., one module, is determined empirically.

Concentration polarization is undesirable for three reasons (9). First, osmotic pressure near the membrane surface is increased. Since the solvent flux, Eq. (3), is proportional to the pressure gradient across the membrane, increasing the osmotic pressure will cause a decline in solvent flux. The second effect of concentration polarization is an increase in the solute concentration at the membrane wall. This increases the concentration driving force across the membrane and, as predicted by Eqs. (3) and (4), increases the solute flux through the membrane. The third effect of concentration polarization is possible membrane fouling. When the concentration of solute species (at the membrane wall) is greatly increased, solute

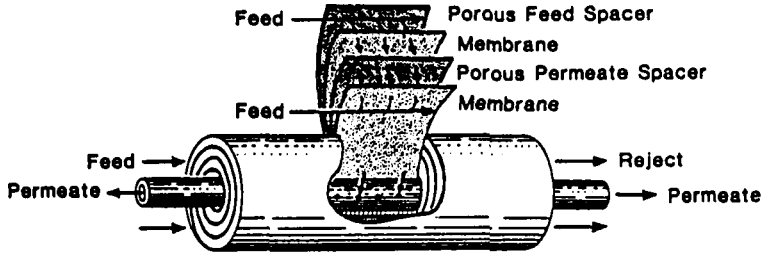

FIG. 2. Spiral wound membrane module configuration (from Ref. 10).

can precipitate onto the membrane surface. This can result in the membrane becoming plugged or coated. Membrane fouling is a complex phenomenon often caused by interactions of various foulants with one another and the membrane.

SYSTEM MODEL

Membrane Operation

A simple lab or pilot scale reverse osmosis system can be operated in several modes. In a large-scale application, feed enters the membrane module, the purified permeate is collected, and the more concentrated retentate is fed to a subsequent membrane module. Each susbsequent membrane "sees" a constant and more concentrated feed.

In a batch, unsteady-state mode of operation (Figure 3), as was the basis for the simulation models, the retentate is recycled to the feed tank and permeate is collected in the product tank. This process is essentially a closed-loop concentrating system using an initial feed volume and concentration. The product permeating the membrane at any instant is called the permeate, while the permeate collected in the permeate/product tank, over a span of time, is called the average permeate.

As the volume of permeate increases in the product tank, the volume in the feed tank decreases. The net result is a lesser volume of more concentrated feed. This type of operation allows the system to be studied at varying levels of feed concentration. Large-scale operation can thus be simulated in a single run. As feed volume diminishes and concentration increases, the system will operate as if it were running in sequential increments of increasing concentration. At some point the system must be

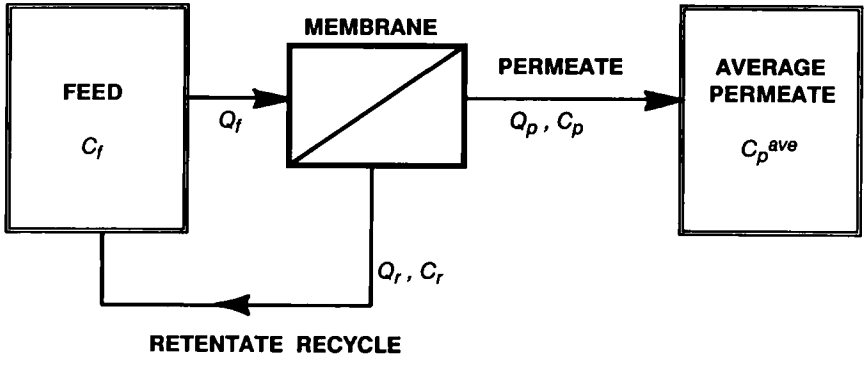

FIG. 3. Closed-loop reverse osmosis concentration system.

stopped because the feed becomes so concentrated that flux drops significantly. This is due to a large increase in osmotic pressure on the feed side, and an increase in problems associated with concentration polarization, at elevated concentrations.

Model Development

Solution diffusion models have been used in the modeling of reverse osmosis systems by Slater et al. (*3*). The focus of the work presented in this paper is the enhancement of the model proposed earlier by the above; the development which follows parallels that of the above. Attention has been placed on representing the feed-side concentration more precisely. Specifically, the feed concentration has been represented as the average of the feed and retentate concentrations. Concentration polarization has also been examined.

As already alluded to, a systems model must be developed since theoretical models for the mass transfer for complex membrane configurations are difficult to develop and utilize. Therefore, the membrane module is represented as a "black box" around which stream concentrations and flows are used. The development of a concentration driving force is based on average values inside the module with an attempt to express the effects of concentration polarization in terms of a module polarization coefficient. This is analogous to an overall heat transfer coefficient in heat exchangers and is explained in more detail later.

The simulation model uses basic transport equations, Eqs. (3) and (4), to depict mass transfer through the membrane. The mass transfer coefficients used in these models were determined experimentally (*3*). Correlations of flux, recovery, and solute concentrations with operating time are presented. Operational characteristics of the system can also be predicted at various times and recoveries. The effects of pressure, feed concentration, volume, and rate as well as membrane characteristics can also be described.

The differential equation representing the change in feed concentration with time is

$$\left(\frac{dC_f}{dt}\right) = \frac{Q_p(C_f - C_p)}{V_f^0 - (Q_p)t} \tag{12}$$

This is the result of material balances on the feed tank, permeate/product tank, and membrane module. A full development of Eq. (12) is given by Slater et al. (*3*). The solution of Eq. (12) requires Q_p and C_p as functions of C_f.

The solvent flux is a function of the osmotic pressure as given by Eq. (3). The relationship between osmotic pressure and solute concentration is given by the Van't Hoff expression

$$\pi = \phi(n/v)R_gT \tag{13}$$

where ϕ is an osmotic pressure coefficient. Molar concentration is given by (n/v), and R_g and T are the universal gas constant and absolute temperature, respectively. It is often convenient to incorporate the constant in Eq. (13), at a constant temperature, into an osmotic pressure to solute concentration coefficient, ψ. The relation becomes

$$\pi = \psi C \tag{14}$$

The value is then assumed to be constant for the particular experimental conditions studied. Using the osmotic pressure, solute concentration relationship in Eq. (14), the solvent flux can be defined as

$$J_w = A_w(\Delta P - \psi \Delta C) \tag{15}$$

In principle, ΔC is the difference between the boundary layer (wall) concentration on the feed side and the permeate concentration, as related in Eq. (5):

$$\Delta C = C_f^w - C_p \tag{5}$$

The wall concentration must be obtained by a mass transfer relationship. This can be determined for simple geometries, i.e., tubular membranes, knowing the process conditions. For more complex geometries, such as the spiral-wound configuration, this is a difficult task, so a general relationship for the entire module is proposed. This relationship would involve the concentrations entering and exiting the module. For simplicity, the feed concentration at the wall is often considered to be that of the bulk feed. To simplify the mathematics, this was first represented by equating the average feed concentration at the wall with the feed concentration entering the membrane module (*3*):

$$C_f^w = C_f \tag{16a}$$

The bulk feed concentration, C_f, can be estimated better by using an average of the feed concentration entering and the retentate concentration

leaving:

$$C_f^w = \frac{C_f + C_r}{2} \tag{16b}$$

This accounts for the increase in concentration as seen in the retentate leaving. This representation of the bulk feed concentration in a spiral-wound membrane module (Fig. 2) yields

$$\Delta C = \frac{C_f + C_r}{2} - C_p \tag{16c}$$

where $(C_f + C_r)/2$ is the average solute (bulk) concentration on the feed side of the membrane and C_p is the permeate concentration. Substitution of Eq. (16c) into Eqs. (4) and (15) yields

$$J_s = B_s\left(\frac{C_f + C_r}{2} - C_p\right) \tag{17}$$

and

$$J_w = A_w\left[\Delta P - \psi\left(\frac{C_f + C_r}{2} - C_p\right)\right] \tag{18}$$

The relationship between solute and solvent flux is given by

$$J_w/C_w = J_s/C_p \tag{19}$$

Substituting Eqs. (17) and (18) into Eq. (26) yields

$$B_s C_w\left(\frac{C_f + C_r}{2} - C_p\right) = C_p A_w\left[\Delta P - \psi\left(\frac{C_f + C_r}{2} - C_p\right)\right] \tag{20}$$

Production rate, Q_p, can be written by combining Eqs. (2b) and (18):

$$Q_p = \frac{S_a}{C_w} A_w\left[\Delta P - \psi\left(\frac{C_f + C_r}{2} - C_p\right)\right] \tag{21}$$

A material balance on the membrane module can be rearranged to yield an expression for the retentate concentration, C_r:

$$C_r = \frac{Q_f C_f - Q_p C_p}{Q_f - Q_p} \tag{22}$$

Equation (20) can also be solved for C_r as a function of C_p and C_f:

$$C_r = \frac{C_p + (z_1 - C_f)C_p - z_2 C_f}{z_2 + C_p} \tag{23}$$

where

$$z_1 = \frac{\Delta p}{\psi} + \frac{B_s C_w}{\psi A_w}, \qquad z_2 = \frac{B_s C_w}{2} A_w$$

Equation (21) can be solved for Q_p as a function of C_p, C_f, and C_r:

$$Q_p = 2z_4 C_p - z_4 C_f - z_4 C_r + z_3 \tag{24}$$

where

$$z_3 = \frac{S_a A_w \Delta P}{C_w}, \qquad z_4 = \frac{S_a A_w \psi}{2C_w}$$

Combining Eqs. (23) and (24) and eliminating C_r yields

$$Q_p = 2z_4 C_p - z_4 C_f + z_3 + \left(\frac{-z_4 C_p - z_5 C_p + z_6 C_p + z_7 C_f}{z_2 + C_p} \right) \tag{25}$$

where

$$z_5 = z_1 z_4, \qquad z_6 = 0.5 z_4, \qquad z_7 = z_2 z_4$$

Combining Eqs. (22) and (25) and eliminating Q_p yields

$$C_r = \frac{-z_8 C_p + z_9 C_f C_p + z_{10} C_f}{z_9 C_p + z_{11}} \tag{26}$$

where

$$z_8 = z_2 z_3, \qquad z_9 = 0.5Q_f, \qquad z_{10} = z_2 Q_f, \qquad z_{11} = z_{10} - z_8$$

Combining Eqs. (23) and (26) and eliminating C_r yields

$$C_p^3 + (x_1)C_p^2 + (x_2)C_p - (x_3) = 0 \tag{27}$$

where

$$x_1 = \frac{n_2 - n_1 C_f}{n_1}, \qquad x_2 = \frac{n_3 - n_4 C_f}{n_1}, \qquad x_3 = \frac{n_5 C_f}{n_1}$$

and

$$n_1 = z_9, \qquad n_4 = z_2 z_9 + 0.5 z_{11} + 0.5 z_{10}$$

$$n_2 = z_1 z_9 + z_{11} + 0.5 z_8, \qquad n_5 = z_2 z_{11} + z_2 z_{10}$$

$$n_3 = z_1 z_{11} + z_2 z_8$$

Model Solution

The solution of the model requires the simultaneous solution of Eqs. (12), (25), and (27):

$$\left(\frac{dC_f}{dt}\right) = \frac{Q_p(C_f - C_p)}{V_f^0 - (Q_p)t} \tag{12}$$

$$Q_p = 2z_4 C_p - z_4 C_f + z_3 + \left(\frac{-z_4 C_p^2 - z_5 C_p + z_6 C_p + z_7 C_f}{z_2 + 0.5 C_f}\right) \tag{25}$$

$$C_p^3 + \left(\frac{n_2 - n_1 C_f}{n_1}\right) C_p^2 + \left(\frac{n_3 - n_4 C_f}{n_1}\right) C_p - \left(\frac{n_5 C_f}{n_1}\right) = 0 \tag{27}$$

where Eqs. (25) and (27) provide the relationships between C_p and C_f, and Q_p and C_f, required for the solution of Eq. (12). Equation (12) is a nonlinear differential equation which has been solved by using the classical fourth-order Runge–Kutta method. Equation (27) is cubic in C_p and was solved by using the Newton method.

Simultaneous solution of Eqs. (12), (25), and (27) yields values for the feed and permeate concentrations, and the permeate flow. From equations already presented, the values of retentate concentration Eq. (22) and solvent flux Eq. (18) can be determined. In addition, the value describing the system's performance can be determined. Specifically, these are the concentration factor Eq. (6), the recovery Eq. (7), and the rejection Eq. (8).

One final relation of interest is the total production permeate concentration, or the average concentration in the permeate tank after a period of operation. The concentration of the permeate tank is equal to the total mass of solute in the tank divided by the total volume of permeate in the tank:

$$C_p^{\text{ave}} = M^{\text{total}}/V^{\text{total}} \tag{28}$$

The total mass is given by

$$M^{\text{total}} = \int Q_p C_p dt = \Sigma Q_p C_p \Delta t \tag{29}$$

and the total volume is given by

$$V^{\text{total}} = \int Q_p dt = \Sigma Q_p \Delta t \tag{30}$$

where Q_p and C_p are functions of t. The simulation program determines these values by performing the above summations.

EXPERIMENTAL

Model Testing

Experimental data were used in testing the model. The data were collected by using the system to purify a simple aqueous salt (NaCl) solution. The experimental system used in this study can accommodate many types of membranes (*11*, *12*). A FilmTec FT-30, SW30-2521, spiral-wound, thin-film composite membrane with a total surface area of 10 ft^2 was used. The process conditions common to all experiments are summarized in Table 1. Figures 4, 5, and 6 represent the simulation data for the three experiments. The points represent the experimental data. The dashed-line curve (labeled old) represents the simulation as earlier proposed, and the solid-line curve (labeled new) represents the new simulation as developed in this work.

The initial conditions and constants for Experiment 1 (Expt. 1) are presented in Table 2 and the relationships are displayed in Figs. 4a–d. The

TABLE 1
Process Conditions for the Reverse Osmosis Experiments

Temperature, T		25°C
Applied pressure gradient, ΔP		600 psi
Feed rate, Q_f		3.0 gpm
Initial feed concentration, C_f^0:	Expt 1	5,000 mg/L
	Expt 2	10,000 mg/L
	Expt 3	20,000 mg/L

first graph, Fig. 4a, shows the recovery as a function of time. A recovery of 99% was achieved after 4.05 h. The graph of flux vs time (Fig. 4b) shows the flux decreasing, as expected, due to an increase in the osmotic pressure of the feed and concentration polarization. Both models predict higher values for the flux than those experimentally measured; the new simulation agrees within 12%. The graph of feed concentration vs time (Fig. 4c) shows C_f increasing from 5000 to over 33,000 mg/L; this is in good agreement with the experimental data. The graph of permeate concentration vs time (Fig. 4d) shows C_p increasing from 16.8 to slightly over 200 mg/L. The model gives values slightly lower for C_p than those experimentally measured; the simulations initially agree with experimental data and deviate at the end of the experiment (high recovery/processing time).

The initial conditions and constants for Experiment 2 (Expt. 2) are presented in Table 3 and the experimental results are shown graphically in Figs. 5a–d. When the feed concentration is increased to 10,000 mg/L, the two simulations deviate more. The graph of recovery vs time (Fig. 5a) shows it now takes 5.85 h to achieve a recovery of 99% compared to the previous 4.05 h. As before, the same trends of decreasing flux (Fig. 5b) and increasing feed and permeate concentrations (Figs. 5c and d) with process time are exhibited. The prediction of feed concentration is still the most accurate.

TABLE 2
Initial Feed Conditions and Parameters for Experiment 1

C_f^0	5000 mg/L
V_f^0	40.33 gal
Q_f	3.0 gpm
ΔP	600 psi
A_w	0.05306 gfd/psi
B_s	9.8431×10^{-8} gfd/mg/L
ψ	0.0114 psi/mg/L

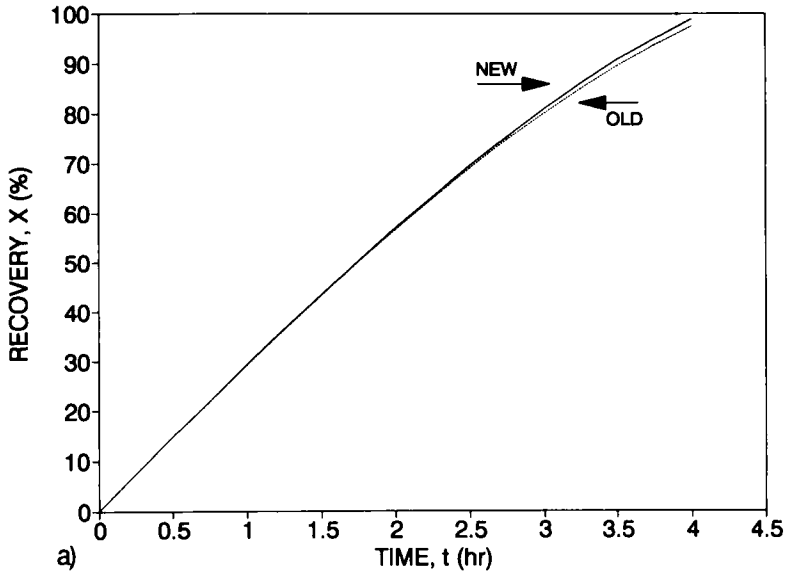

FIG. 4a. Recovery (%) vs processing time (h) for Experiment 1 using an initial feed concentration of 5000 mg/L. Simulation results for the new model (——) and the earlier model (- - -) (*3*).

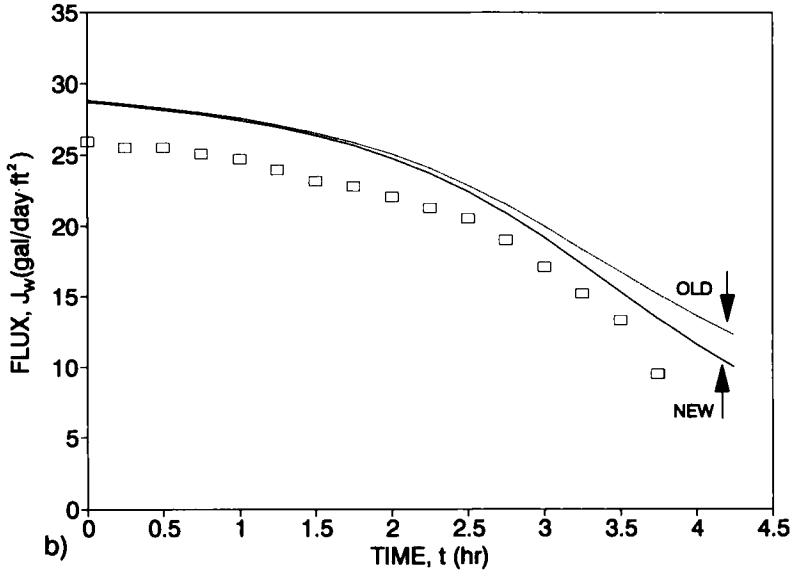

FIG. 4b. Flux (gal/day·ft²) vs processing time (h) for Experiment 1 using an initial feed concentration of 5000 mg/L. Simulation results for the new model (——), earlier model (- - -) (*3*), and experimental results (□).

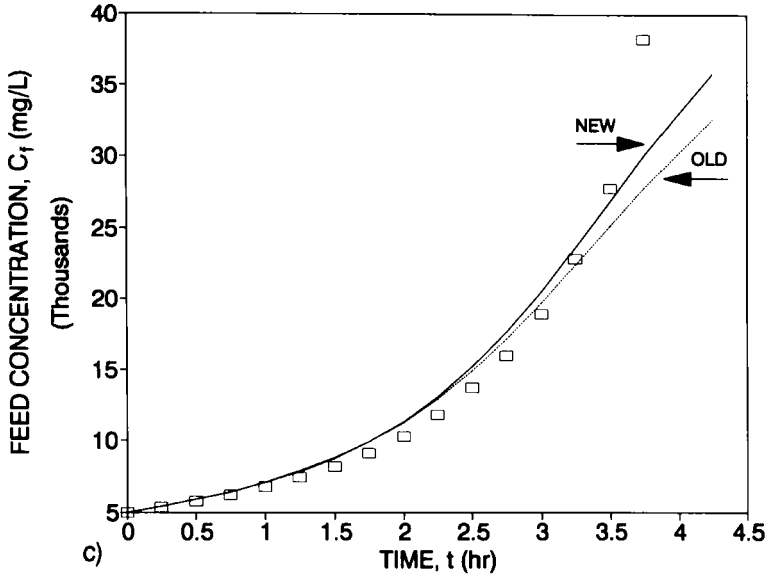

FIG. 4c. Feed concentration (mg/L) vs processing time (h) for Experiment 1 using an initial feed concentration of 5000 mg/L. Simulation results for the new model (——), earlier model (- - -) (*3*), and experimental results (□).

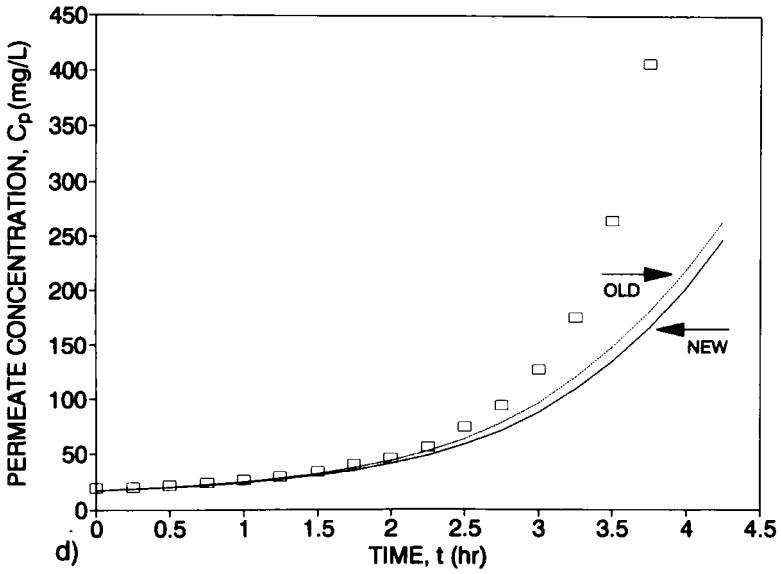

FIG. 4d. Permeate concentration (mg/L) vs processing time (h) for Experiment 1 using an initial feed concentration of 5000 mg/L. Simulation results for the new model (——), earlier model (- - -) (*3*), and experimental results (□).

TABLE 3
Initial Feed Conditions and Parameters for Experiment 2

C_f^0	10,000 mg/L
V_f^0	39.89 gal
Q_f	3.0 gpm
ΔP	600 psi
A_w	0.05306 gfd/psi
B_s	11.157×10^{-8} gfd/mg/L
ψ	0.0114 psi/mg/L

The initial conditions and constants for Experiment 3 (Expt. 3) are presented in Table 4 and the experimental results are shown graphically in Figs. 6a–d. The highest initial feed concentration studied was 20,000 mg/L. Here the effects of concentration polarization and potential fouling are greatest and the deviations between the two simulations are largest. The simulation as originally proposed shows an abrupt ending due to the model predicting a negative flux. Although the original simulation has this

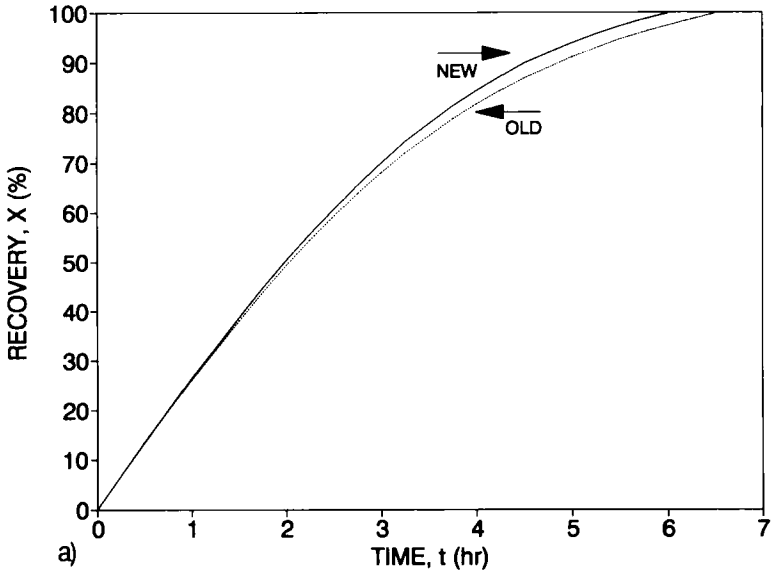

FIG. 5a. Recovery (%) vs processing time (h) for Experiment 2 using an initial feed concentration of 10,000 mg/L. Simulation results for the new model (——) and the earlier model (- - -) (*3*).

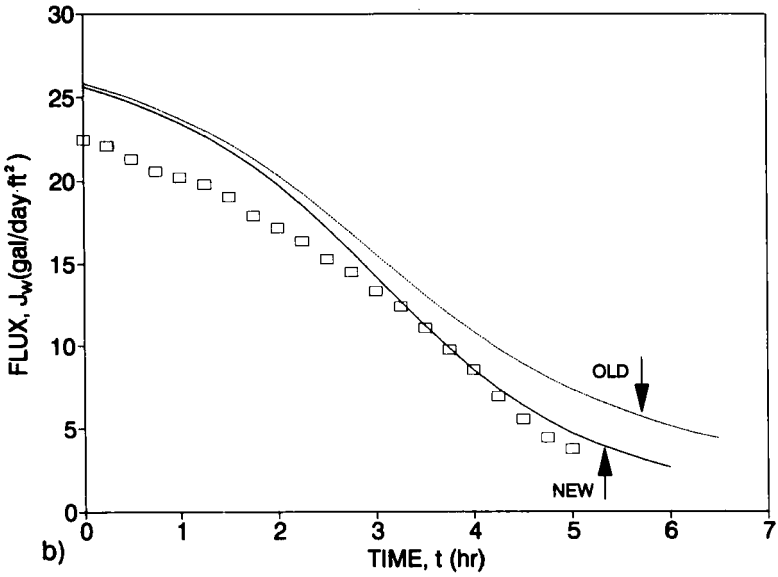

FIG. 5b. Flux (gal/day·ft^2) vs processing time (h) for Experiment 2 using an initial feed concentration of 10,000 mg/L. Simulation results for the new model (——), earlier model (- - -) (*3*), and experimental results (□).

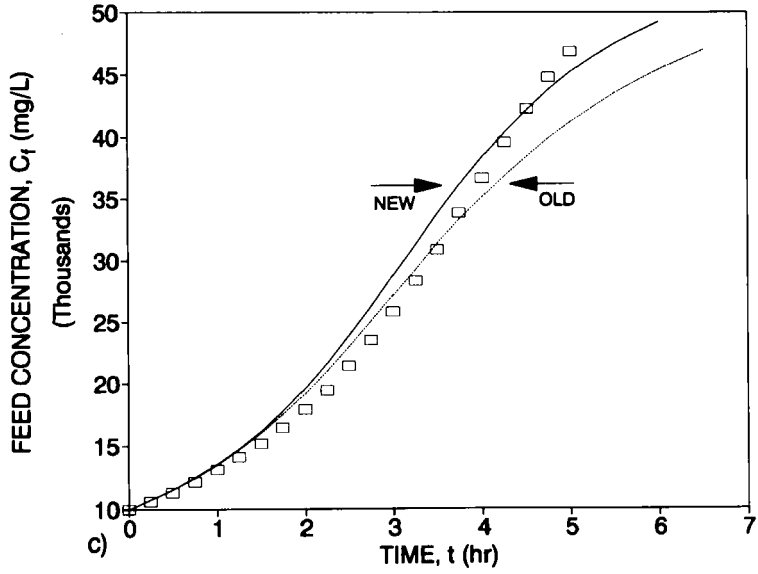

FIG. 5c. Feed concentration (mg/L) vs processing time (h) for Experiment 2 using an initial feed concentration of 10,000 mg/L. Simulation results for the new model (——), earlier model (- - -) (*3*), and experimental results (□).

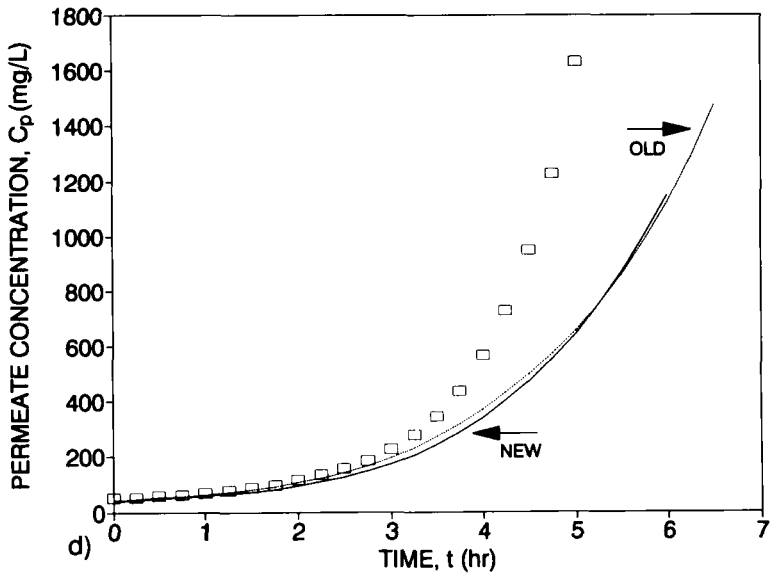

FIG. 5d. Permeate concentration (mg/L) vs processing time (h) for Experiment 2 using an initial feed concentration of 10,000 mg/L. Simulation results for the new model (——), earlier model (- - -) (*3*), and experimental results (□).

anomaly, the predicted values do show agreement with the experimental data. The difference between the two models is still relatively small, suggesting that either one can be used with good results.

It should be noted that the models do not account for the actual feed concentration at the membrane surface or wall. In addition, the models are very sensitive to the values of B_s and A_w, which were empirically determined.

TABLE 4
Initial Feed Conditions and Parameters for Experiment 3

C_f^0	20,000 mg/L
V_f^0	39.56 gal
Q_f	3.0 gpm
ΔP	600 psi
A_w	0.05306 gfd/psi
B_s	13.91×10^{-8} gfd/mg/L
ψ	0.0114 psi/mg/L

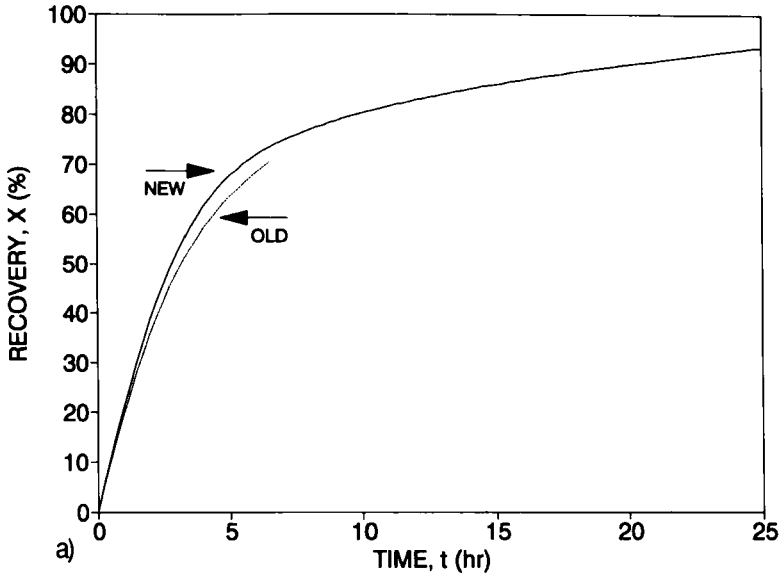

FIG. 6a. Recovery (%) vs processing time (h) for Experiment 3 using an initial feed concentration of 20,000 mg/L. Simulation results for the new model (——) and the earlier model (- - -) (*3*).

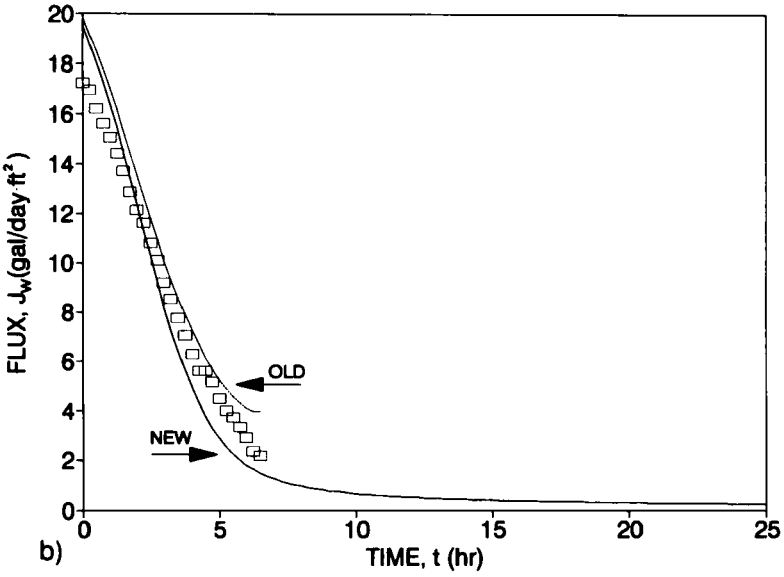

FIG. 6b. Flux (gal/day·ft^2) vs processing time (h) for Experiment 3 using an initial feed concentration of 20,000 mg/L. Simulation results for the new model (——), earlier model (- - -) (*3*), and experimental results (□).

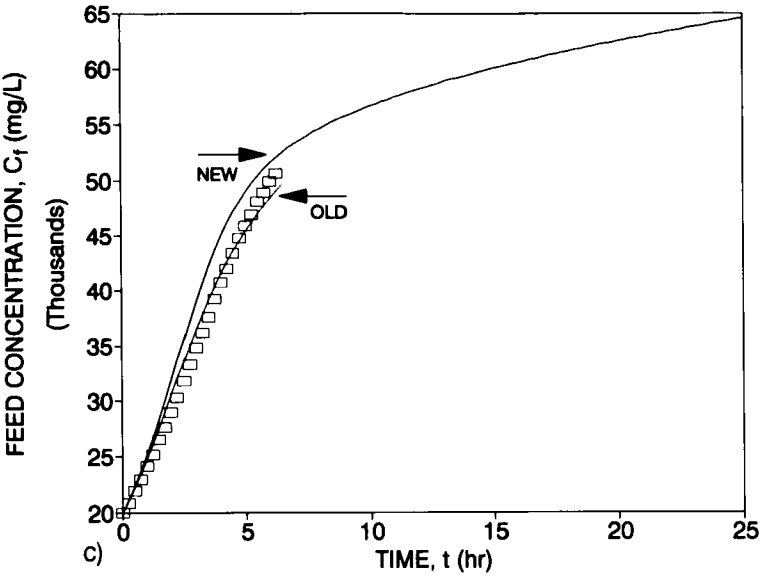

FIG. 6c. Feed concentration (mg/L) vs processing time (h) for Experiment 3 using an initial feed concentration of 20,000 mg/L. Simulation results for the new model (——), earlier model (- - -) (*3*), and experimental results (□).

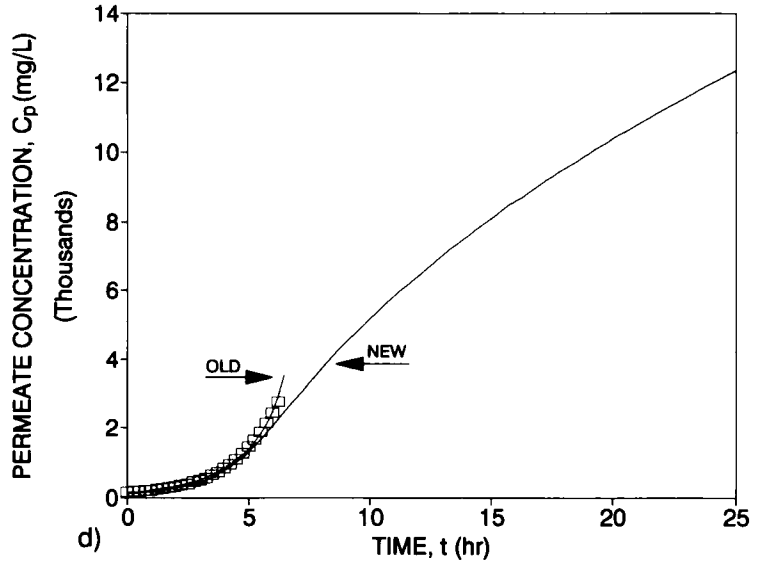

FIG. 6d. Permeate concentration (mg/L) vs processing time (h) for Experiment 3 using an initial feed concentration of 20,000 mg/L. Simulation results for the new model (——), earlier model (- - -) (*3*), and experimental results (□).

Concentration Polarization Coefficient

In an attempt to incorporate the effects of concentration polarization, a concentration polarization coefficient for the overall module, θ, was developed. This can be expressed as the ratio of the concentration gradient at the wall to the gradient in terms of the bulk concentrations.

$$\theta = \frac{C_f^w - C_p}{C_f^b - C_p} \tag{31}$$

Applying this to the basic transport equations, Eqs. (4) and (15),

$$J_s = B_s \Delta C \tag{4}$$

$$= B_s \theta \Delta C \tag{4a}$$

$$J_w = A_w(\Delta P - \psi \Delta C) \tag{15}$$

$$= A_w(\Delta P - \psi \theta \Delta C) \tag{15a}$$

where

$$\Delta C = \frac{C_f^w - C_p}{C_f^b - C_p}(C_f^b - C_p) = C_f^w - C_p \tag{32}$$

In this way Eqs. (4a) and (15a) are expressed in terms of the wall concentration. Likewise, a polarization coefficient could be expressed as the ratio of the concentration of the feed at the wall to the concentration in the bulk feed. This is the quantifying relationship already presented.

$$\theta' = C_f^w / C_f^b \tag{33}$$

The polarization coefficient is important because it gives a quantitative measure of the actual concentrations in the system.

Experimental data were used to calculate the value of the polarization coefficient. The concentration gradient, ΔC, can be calculated from Eq. (15). This value is the concentration gradient which results in the measured solvent flux J_w. Knowing the concentration of the retentate allows the feed concentration at the wall to be calculated:

$$\Delta C = C_f^w - C_r \quad \text{or} \quad C_f^w = \Delta C + C_r$$

The calculated values of θ and θ' from Expt. 1 are plotted vs the feed concentration in Fig. 7. The graph shows the two expressions for the polarization coefficient give almost identical results, with θ decreasing as the feed concentration increases.

The graph in Fig. 8 represents the calculated values of θ and θ' from Expt. 3. The decrease in the polarization coefficient is still observed, but with much less significance. Figure 9 shows the results of the three experiments plotted together. The composite graph suggests a general trend of decreasing polarization with increasing feed concentration. This can be explained by examining the relationship between the solvent flux and the polarization coefficient.

A composite graph of the polarization coefficient vs the solvent flux appears in Fig. 10. The polarization coefficient increases with increasing solvent flux. At low solvent fluxes, solute species more readily diffuse away from the membrane. Conversely, high fluxes allow the solute species to

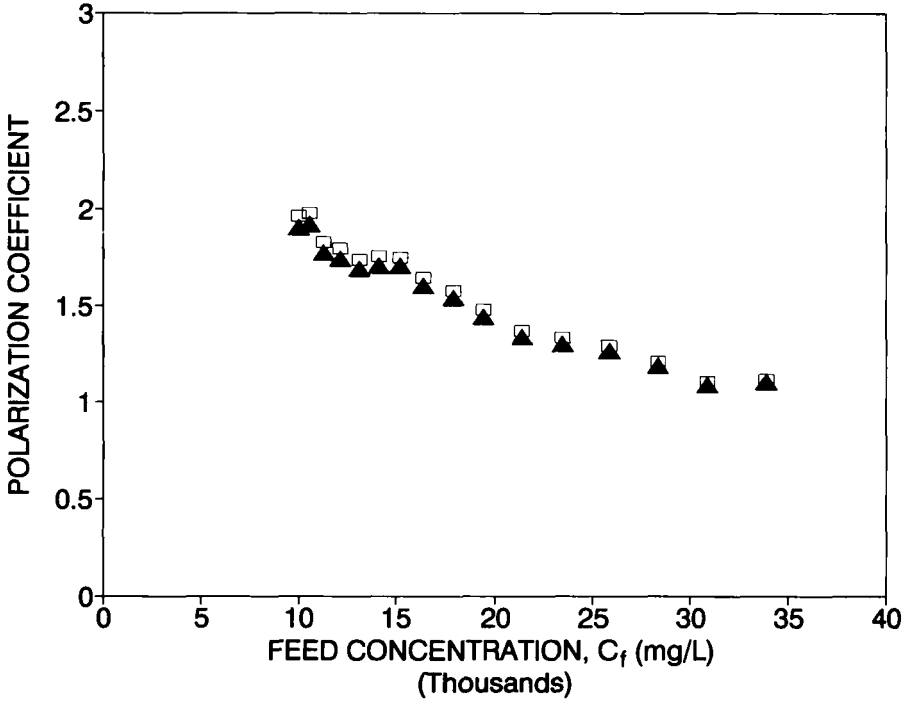

FIG. 7. Concentration polarization coefficients (dimensionless) vs feed concentration (mg/L) for Experiment 1. Polarization coefficient, θ' (□); polarization coefficient, θ (▲).

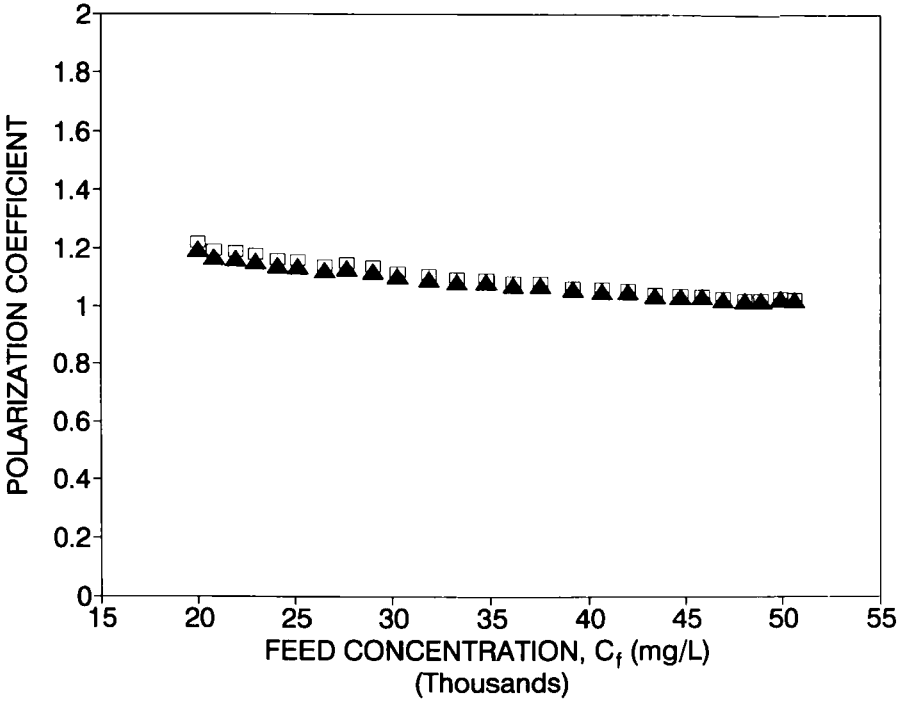

FIG. 8. Concentration polarization coefficients (dimensionless) vs feed concentration (mg/L) for Experiment 3. Polarization coefficient, θ' (□); polarization coefficient, θ (▲).

be convectively carried to the membrane surface. As a result, the solute species are polarized on the membrane.

The relationship between the polarization coefficient and feed concentration can thus be attributed to the solvent flux. When the concentration of the feed is increased, the solvent flux decreases. Therefore, the decrease of the polarization coefficient results from this lowering of the flux. This suggests that the polarization coefficient is more directly related to the solvent flux.

CONCLUSIONS

The development of a simulation model has been presented and compared to previously proposed models. Prior work uses the bulk feed concentration to represent the actual wall concentration; the model developed in this work uses the average of the bulk feed and bulk retentate. The simulations incorporate material balances on the system and solution dif-

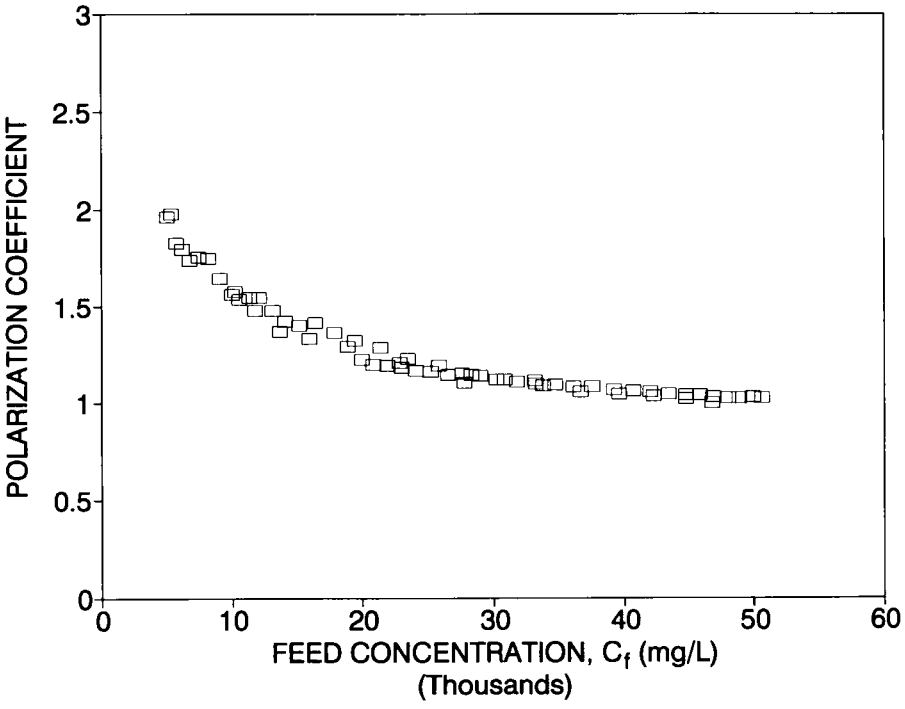

FIG. 9. Composite graph of concentration polarization coefficients (dimensionless) vs feed concentration (mg/L) for Experiments 1, 2, and 3.

fusion mass transfer models. The simulations show excellent agreement when predicting feed concentration. The prediction of permeate flux is within 15% (for both models), and the values predicted for the permeate concentration are initially very good but deviate significantly over the period of the experimental study. The comparison of the two suggests that the models do not deviate significantly enough to justify the more cumbersome solution developed in this work.

A polarization coefficient has been used to more accurately represent the actual wall concentrations. The polarization coefficient was found to depend on the solvent flux, and it increased as the flux increased. The preliminary correlation of the polarization coefficient with solvent flux suggests that an empirical relation between θ and J_w can be developed. Such a relationship can then be applied to a modified mass transfer expression, and a simulation model more accurately representing system concentrations can be used.

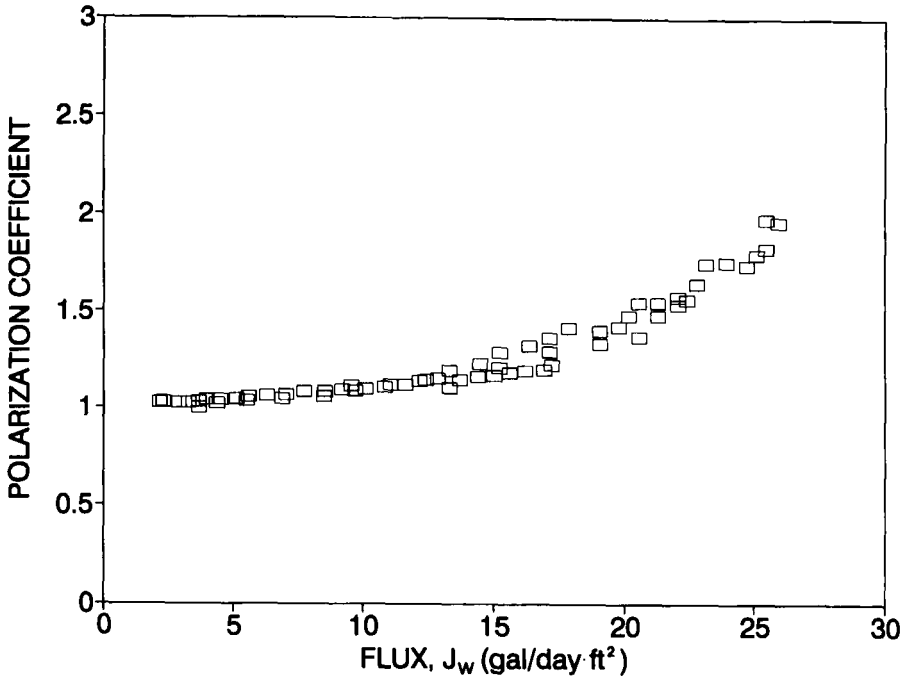

FIG. 10. Composite graph of concentration polarization coefficients (dimensionless) vs flux (gal/day·ft²) for Experiments 1, 2, and 3.

Acknowledgments

Partial support for this work was provided by grants from the Exxon Educational Foundation and the National Science Foundation (USE #8551851).

NOMENCLATURE

A_w	solvent permeability coefficient
B_s	solute permeability coefficient
C	concentration
C_d	solvent concentration
C_f	feed solute concentration
C_f^b	feed bulk solute concentration
C_f^w	feed boundary-layer wall concentration
C_f^0	initial solute concentration of feed
C_p^{ave}	overall production permeate solute concentration
C_p	permeate solute concentration
C_r	retentate solute concentration

CF	concentration factor (dimensionless)
D	diffusion coefficient of solute in solvent
J_s	solute mass flux
J_w	solvent, permeate mass flux
J'_w	solvent, permeate volume flux
l	boundary layer thickness
M^{total}	total mass of solute
n	moles of solute
n_1–n_5	simulation model parameters
ΔP	applied transmembrane pressure
Q_f	volumetric flow rate of feed
Q_p	volumetric flow rate of permeate
Q_r	volumetric flow rate of retentate
R	solute rejection
R	universal gas constant
R_i	intrinsic solute rejection
t	processing time
T	temperature
u_b	feed velocity parallel to membrane
v	volume of solvent
V_p	volume of permeate
V_f^0	initial volume of feed
V_f	volume of feed
V^{total}	total volume of permeate produced
X	overall batch volumetric recovery
x_1–x_3	simulation model parameters
Y	single pass volumetric recovery
z_1–z_{11}	simulation model parameters
π	solute osmotic pressure
ϕ	osmotic pressure coefficient
θ, θ'	concentration polarization coefficients
ψ	osmotic pressure to solute concentration ratio

REFERENCES

1. S. A. Leeper, D. H. Stevenson, P. Y. C. Chiu, S. J. Priebe, H. F. Sanchez, and P. M. Wilkoff, *Membrane Technology and Applications: An Assessment,* EG & G Idaho, Inc., Idaho Falls, Idaho, 1984.
2. C. S. Slater, R. C. Ahlert, and C.G. Uchrin, *Desalination, 48,* 171 (1983).
3. C. S. Slater, J. Zielinski, R. G. Wendel, and C. G. Uchrin, *Ibid., 52,* 268 (1985).
4. R. Rautenbach and R. Albrecht, *Membrane Processes,* Wiley, New York, 1989 Chap. 10.
5. S. T. Hwang and K. Kammermeyer, *Membranes in Separations,* Krieger, Malabar, Florida, 1984.

6. M. Mulder, *Basic Principles of Membrane Technology,* Kluwer, Dordrecht, The Netherlands, 1991.
7. S. Sourirajan and T. Matsuura, *Reverse Osmosis/Ultrafiltration Process Principles,* (NRCC No. 24188), National Research Council of Canada, Ottawa, Canada, 1985.
8. P. M. Bungay, H. K. Lonsdale, and M. N. de Pinho (eds.), *Synthetic Membranes: Science, Engineering and Applications,* Reidel, Dordrecht, The Netherlands, 1986.
9. D. E. Potts, R. C. Ahlert, and S. S. Wang, *Desalination, 36,* 239 (1981).
10. J. L. Bravo, J. R. Fair, J. L. Humphrey, C. L. Martin, A. F. Seibert, and S. Joshi, *Assessment of Potential Energy Savings in Fluid Separation Technologies* (DE85013839), University of Texas at Austin, Austin, Texas, 1985.
11. C. S. Slater and J. D. Paccione, in *Proceedings of the 1986 Annual Conference of the American Society for Engineering Education,* 1986, p. 812.
12. C. S. Slater and J. D. Paccione, *Chem. Eng. Educ., 22,* 138 (1987).

Received by editor September 30, 1991
Revised February 18, 1992